J Electroceram (2007) 19:81–94
DOI 10.1007/s10832-007-9045-2

Nanoscale characterization of polycrystalline ferroelectric materials for piezoelectric applications

A. L. Kholkin · I. K. Bdikin · D. A. Kiselev · V. V. Shvartsman · S.-H. Kim

Received: 22 August 2006 / Accepted: 11 December 2006 / Published online: 6 March 2007

Abstract In this work, the nanoscale electromechanical properties of several important piezoelectric materials [as exemplified by $PbZr_xTi_{1-x}O_3$ (PZT)] suitable for both bulk actuator and microelectromechanical system (MEMS) applications are reported. The investigations are performed by the piezoresponse force microscopy (PFM) that is currently the most suitable tool for both ferroelectric domain imaging and local piezoelectric studies. The local piezoresponse of individual grains is measured in PZT films and compared with average piezoelectric behavior. Frequency dependencies of local piezoelectric coefficients are presented and analyzed. The results on local piezoelectric nonlinearity, as well as on nanoscale fatigue and aging are briefly discussed. These measurements demonstrate that PFM is promising for studying local piezoelectric phenomena in polycrystalline ferroelectrics where defects and other inhomogeneities are essential for the interpretation of macroscopic piezoelectric properties. Finally, local electromechanical properties of polycrystalline relaxors (PMN-PT, PLZT, doped $BaTiO_3$) are briefly outlined.

Keywords Piezoelectricity · Ferroelectricity · Relaxors · Piezoresponse force microscopy · Local properties

A. L. Kholkin (✉) · I. K. Bdikin · D. A. Kiselev
Department of Ceramics and Glass Engineering,
CICECO, University of Aveiro,
3810-193 Aveiro, Portugal
e-mail: kholkin@cv.ua.pt

V. V. Shvartsman
Department of Physics, University of Duisburg-Essen,
47048 Duisburg, Germany

S.-H. Kim
INOSTEK Inc., Gyeonggi Technopark,
Ansan, Gyeonggi 426-901, South Korea

1 Introduction

The science and technology of ferroelectrics is nowadays attracting a surge of interest because of the large number of applications envisaged in the nearest future. These include nonvolatile memories, microelectromechanical systems (MEMS), optical modulators and waveguides, uncooled pyroelectric detectors, and many others [1].

It is important that, using modern deposition and patterning techniques, ferroelectrics can be integrated in Si-based integrated circuits thus allowing novel functional devices to be developed. The word MEMS is normally synonymous with the microfabricated devices comprising mechanical actuator and sensor functions with processing and control electronics on a common substrate. Commercial applications of MEMS include medicine (e.g., blood pressure sensors and micropumps for drug delivery), information technology (e.g., displays), automotive industry (accelerometers), manufacturing (microflow controllers) etc. Their number is increasing every year especially in biological areas. Ferroelectric materials are the main candidates for active elements in MEMS because of their high piezoelectric coefficients, broad frequency range, and fast response [2]. In addition, they do not dissipate power in the static mode and have the highest energy density among all actuator materials. Due to the small size of ferroelectric elements in MEMS, there is a growing need in microscopic techniques allowing for the evaluation of their piezoelectric properties with the nanoscale resolution. Such technique, piezoresponse force microscopy (PFM), became an interesting opportunity for the measurements of local electromechanical properties of ferroelectric films, single crystals, and even ceramics [3–8]. Along with the local measurements of piezoelectric coefficients and domain visualization, this technique allows for a direct matching of local

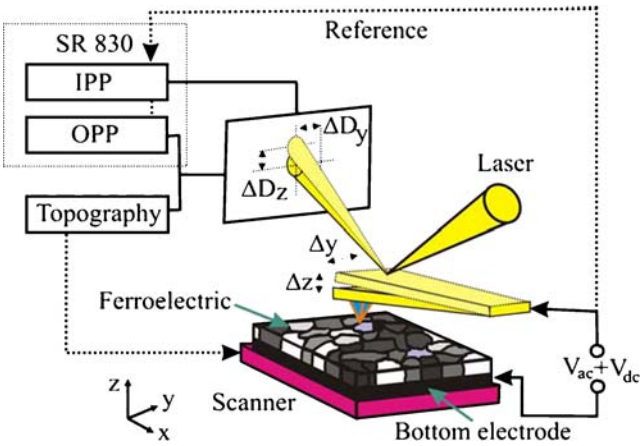

Fig. 1 Schematic of the PFM technique as applied to polycrystalline ferroelectrics

properties to the microstructural details, since both are imaged simultaneously. In addition, local poling and domain writing can be done transforming PFM into a nanoscale memory setup with extremely high density (up to 100 Gb/in^2) [9]. In polycrystalline ferroelectrics, the use of PFM is of prime importance, because complex interactions of domain walls with grain boundaries and defects can be, in principle, visualized. In this work, the PFM technique is applied to a number of ferroelectric polycrystalline materials promising for piezoelectric applications and MEMS. It is shown that the typical piezoelectric behavior is significantly modified at the nanoscale sheding light on the microscopic mechanisms of piezoelectricity in ferroelectrics.

2 Principle of PFM operation

The PFM was developed for the imaging of polarized regions in ferroelectric copolymer films [10] and later was applied for the visualization of domain structure of ferroelectric films [11]. This method is based on the detection of local electromechanical vibrations of ferroelectric sample caused by an external ac field applied between the conducting tip and a counter electrode (Fig. 1). The deflection signal of the cantilever that oscillates together with the surface of the sample is detected using two lock-in amplifiers and is imaged along with the regular topographic signal in the contact mode. The modulation frequency (ω_{ac}) should be much smaller than the resonance frequency of the cantilever (ω_{res}) but much larger than the frequency of the feedback loop (ω_{FB}).

The domain structure is visualized by monitoring the first harmonics of the deflection signal. The amplitude is proportional to the local longitudinal piezoelectric coefficient d_{33} and the phase ϕ reflects the polarization direction (~0° if the field is parallel to polarization and ~180° if it is antiparallel). If the signal with phase is imaged ($d_{33}\cos\phi$), the contrast depends on both the amplitude of d_{33} and polarization direction (see Fig. 2 as an example of the PFM image in a polycrystalline ferroelectric). The bright areas on this image depict polarization directed towards the bottom electrode and dark areas correspond to the domains of opposite direction. The applied voltage has to be high enough in order to cause the measurable signal but it should be sufficiently small to prevent local switching and domain wall motion. Along with vertical deflection of the cantilever, a lateral motion could be detected via the friction force [4]. Since the torsional motion of the cantilever is involved, the ferroelectric must be scanned in two orthogonal directions. Local piezoelectric hysteresis can be measured by the application of series of voltage pulses with variable height and acquiring the piezoelectric signal after each pulse. It is essential that, since the sharp conducting tip is in the direct contact with the film, the lateral resolution is mainly determined by the tip-sample contact area. In addition, due to the large dielectric permittivity of ferroelectrics, the electric field generated by the tip is effectively concentrated just beneath the contact area and decays rapidly with the distance [12]. For doped Si tips used in this study the resolution was estimated to be about 10–25 nm depending on the applied force. The resolution of the method could be verified by measurements on PZT films with high tetragonality (Ti content=0.8) where the regular *a*–*c* domain structure is typically observed. Figure 3 illustrates the domain structure and cross-section of the piezoelectric image over the domain wall that sets an apparent upper limit of the domain wall width of ~10 nm. We believe that the transition from *c*- to *a*-domain is mainly limited by PFM resolution, since the thickness of the 90° domain walls is believed to be significantly smaller than this value. In the following, we will review our recent findings on the PFM characterization of ferroelectric materials focusing on polycrystalline materials for piezoelectric and MEMS applications.

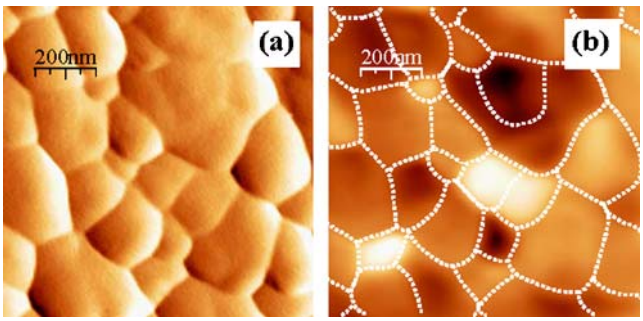

Fig. 2 Topograhy (**a**) and piezoreponse (**b**) images of a sol-gel PZT70/30 film (thickness 4 μm). Grain boundaries are delineated with dotted lines

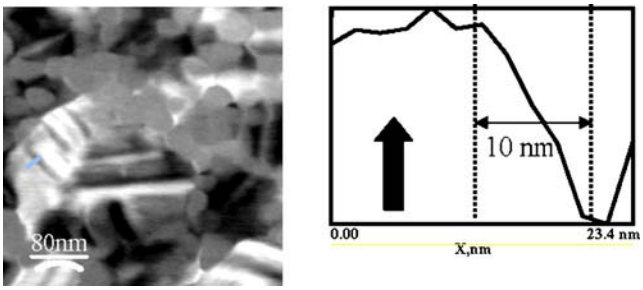

Fig. 3 Piezoelectric image of a PZT(20/80) film (*left*) and cross-section of the piezoelectric signal across the a–c domain boundary illustrating lateral resolution of the PFM technique

3 Local piezoresponse of PZT films

We investigated local piezoelectric maps of polarized PZT films prepared by INOSTEK, Inc. that are commercially fabricated for MEMS applications. Two methods were used for the evaluation of the piezoelectric properties of the films at the nanoscale: in the first experiment, the films were scanned with the voltage +30 V applied to the tip over the area of 2×2 μm^2. Then the averaged piezoelectric response (proportional to $d_{33}\cos\phi$) was plotted as a function of the composition for films of two thicknesses (1 and 4 μm). Only relative values are given as the calibration procedure was not done. The results were compared with macroscopic measurements performed by laser interferometry [20]. In the second mode, hysteresis loops were measured by applying the sequence of voltages to the static tip. The comparison of piezoelectric contrast of films polarized by first method for three investigated compositions is shown in Fig. 4. It is seen that the maximum contrast is observed in PZT48/52 films (x=0.48) in a good accordance with the macroscopic data (http://www.inostek.com). Tetragonal films showed the weakest contrast, however, some grains are seen to be perfectly polarized. It can be understood that relatively poor piezoelectric response of tetragonal films comes mostly from the misalignment of some grains (probably, combined with low polarizability due to size effects). It means that, if proper orientation/uniform grain size is achieved, the films could have much better average piezoelectric properties. On the contrary, almost all grains are polarized to the saturation in the case of the morphotropic phase boundary films (x=0.48). It thus can be concluded that the orientation is not a limiting factor for the d_{33} saturation in the morphotropic phase boundary films. It can be also noted that such obtained local d_{33} (x=0.48) does not depend on thickness, though the macroscopic one apparently does (see, e.g., [13]). This is a natural result of the PFM measurement mode: piezoelectric properties are probed locally (on the film's surface) and clamping effect (that mainly determines d_{33} thickness dependence [13]) is not important.

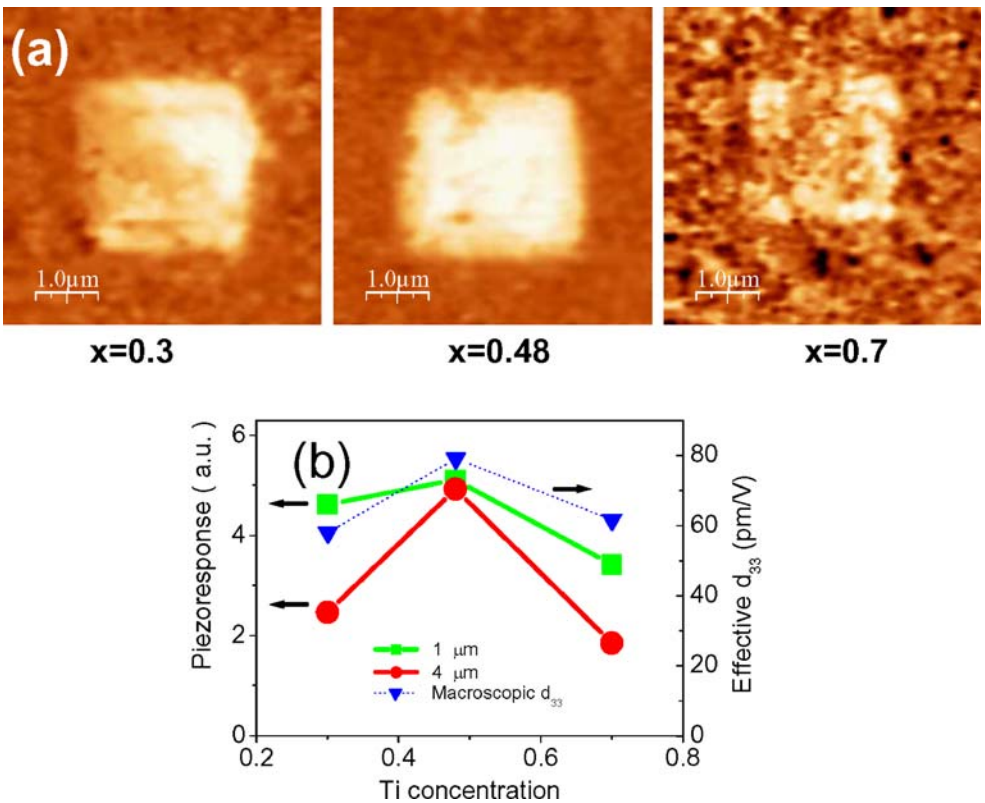

Fig. 4 (**a**)–Piezoimages of locally poled 4 μm thick PZT films of different compositions (V=+30 V) and (**b**) comparison of average local piezoresponse measured on 2×2 μm^2 poled areas with the microscopic values [8]

Another conclusion can be drawn from the analysis of the local piezoelectric properties of rhombohedral films (x= 0.3): 1 μm thick films with (111) texture have much higher local piezoelectric contrast than the 4 μm thick films with (100) orientation. It means that the texture of the rhombohedral films is a major limiting factor influencing their local piezoelectric properties. The same is true for the tetragonal films where 4 μm films with random texture are less piezoelectric than the (111) oriented 1 μm thick films. The results of this analysis differ significantly from that based on macroscopic data where the effect of thickness is more pronounced than the effect of texture. We believed that local poling studies are very important for the establishment of structure-property relationship in ferroelectric films for MEMS.

4 Local hysteresis by PFM

Along with the local poling performed with voltage applied to the tip during scanning, PFM can be used in a spectroscopy mode when the measurements are done on a fixed position of the tip (so-called local d_{33} hysteresis acquisition) with the dc voltage swept in the cyclic manner. This dependence of the local piezoelectric vibration on applied bias is referred to as a piezoresponse hysteresis loop [3]. If performed on a macroscopic scale, this loop corresponds to a weak-field piezoelectric coefficient tuned by a continuously varying bias field. According to a linearized electrostriction equation, the piezoelectric coefficient in ferroelectric films can be often expressed as $d_{33}= 2Q\varepsilon_{33}P_3$ where Q is the effective longitudinal electrostriction coefficient and ε_{33} and P_3 are the corresponding dielectric constant and spontaneous polarization values [14]. Therefore, the d_{33} variation reflects polarization switching with corresponding tuning of the dielectric permittivity $\varepsilon(E)$ and polarization $P(E)$, which both affect piezoelectric coefficient [14]. Piezoelectric hysteresis loops are indeed very useful for the identification of the switching mechanism and ferroelectric degradation both in thin film [15] and bulk ferroelectrics [16]. It should be stressed that, at the nanoscale level, the shape of piezoelectric loop is different [17] reflecting different physical mechanisms involved. Measurements of local hysteresis loops are of great importance in inhomogeneous or polycrystalline ferroelectrics because they are able to quantify polarization switching on a scale significantly smaller than the grain size or inhomogeneity variation (typically few tens of nm). Macroscopically, the switching occurs via the nucleation and growth of a large number of reverse domains in the situation where the applied electric field is uniform. Therefore, the d_{33} hysteresis reflects the switching averaged over entire sample under the electrode. In PFM experimental conditions, the electric field is strongly localized and inhomogeneous, therefore, the polarization switching starts with the nucleation of a single domain just under the tip [18]. Upon increasing the applied dc bias, this newly formed domain elongates to the bottom electrode, simultaneously expanding in lateral dimensions until reaching an equilibrium size, which depends on the value of maximum applied voltage.

The shape of the local piezohysteresis measured by PFM can be understood by scanning the area adjacent to the tip in between the voltage increments, provided no significant relaxation occurs. In addition, useful information on the propagation of domain walls in ferroelectrics can be obtained. An example of the visualization of the piezoelectric hysteresis in polycrystalline PZT films prepared by sol-gel is shown in Fig. 5b [19]. The measurements were done in a cyclic manner, but the switching voltage was periodically interrupted for scanning. The images are shown near the corresponding points of the hysteresis loop.

It is seen that the sudden contrast change (arrow at V^*) corresponds to the appearance of the stable inverse domain. As such, threshold voltage $V^*\approx 11$ V can be considered as an analog of the coercive voltage in local measurements rather than the voltage where $d_{33}=0$ (as in interferometry measurements, see, e.g., [20]). A rapid increase of d_{33} with increasing V_{dc} was explained by the forward and lateral growth of the nucleated domain, progressively contributing to the PFM signal [21, 22] When the size of the inverse domain is much greater than the penetration depth of the weak ac probing field, the tip senses only a fully polarized area with aligned polarization and d_{33} is well saturated. Figure 5a also illustrates the propagation of domain wall in polycrystalline ferroelectrics where local inhomogeneities and stresses make the domain boundary strongly irregular. Thus local hysteresis measurements allow visualization of local stresses and defect agglomerates in polycrystalline ferroelectrics.

Figure 5a represents a comparison of local hysteresis loops measured on PZT films with three different compositions. The representative, sufficiently large grains with uniform contrast were chosen to avoid irreproducibility due to grain size effect and effect of subsurface grains. All films were (111) oriented. The important observation is that the coercive voltages for 1 μm films are approximately the same, while macroscopic coercive fields differ drastically, being much higher for the tetragonal composition (Bdikin, Kholkin, Kim, unpublished). This effect can be easily explained by the distribution of the applied electric field and propagation of the domain of opposite polarity. Indeed, even though the high tetragonal distortion for PZT (x=0.7) should lead to a higher activation energy for this film the threshold voltages are approximately the same for tetragonal and rhombohedral films. It means that lower probability

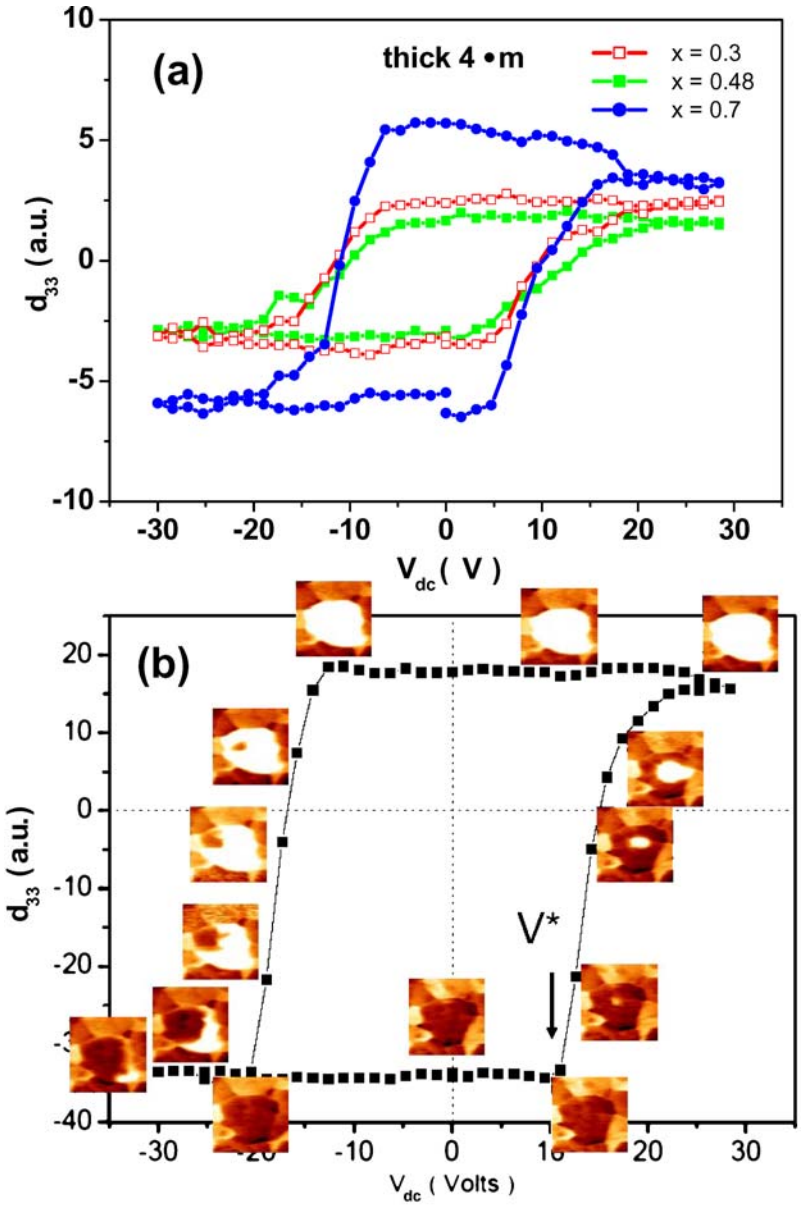

Fig. 5 (**a**) PFM hysteresis loops of films of different Ti content *x*. (**b**) Detailed hysteresis loop of PZT70/30 film with intermediate scanning. The insets (scan size 1 μm) show the static domain structures obtained by scanning with the ac voltage of the amplitude of 1 V in the corresponding points of the hysteresis [19]

of the nucleation of tetragonal domain is probably counteracted by higher electric field at the interface (that apparently increases upon increasing dielectric constant of the material). It is also important that the effective piezoelectric response under the saturation is considerably higher for this film, as opposite to the macroscopic observations [23]. It may be concluded that the local piezoresponse obtained by the hysteresis is similar to the local polarization, rather than the local d_{33}. Again, this happens because the local piezoelectric signal is determined not only by the effective d_{33} under the tip but also by the ratio between the dielectric constants of the interface layer and the film. In tetragonal films with lower dielectric constants, the electric field seen by a ferroelectric is higher than in the morphotropic phase boundary films and this can give rise to an apparent increase of the piezoelectric response measured by PFM.

5 Piezoelectric non-linearity and depinning of domain walls

Piezoelectric nonlinearity is the essential property of ferroelectrics, which piezoelectric response is partly due to the motion of 90° domain walls. It has been previously shown that the piezoelectric nonlinearity is rather weak in the investigated sol-gel PZT films [24, 25] evidencing that the domain wall mobility is limited as compared with that in bulk materials. In our local experiments, we did not expect any appreciable nonlinearity because the piezoelectric

signal was acquired inside homogeneously polarized areas (domains) where no influence of the domain walls was expected. Figure 6 shows typical ac driving voltage dependencies of d_{33} defined as the measured signal divided by the amplitude of driving voltage in PZT45/55 films. The signal is measured inside domains of opposite polarities. "Negative" d_{33} ("dark" domains, phase ~180°) demonstrates rather weak ac-field dependence at low voltages but its absolute value starts to increase at some voltage V_{th}≈2.5 V. Then d_{33} saturates and tends to decrease, most probably due to global polarization switching. When measured in a "bright" domain, the response is quite different: the linear behavior is followed by a gradual decrease of the local piezoelectric coefficient down to a zero signal. Then d_{33} changes the sign at V^*≈4 V and steeply increases up to a value characteristic of the "negative" domain. It is essential that V^* is well below the coercive voltage for global polarization reversal. Thus switching into the opposite polarization state at low voltages is demonstrated. This amplitude instability imposes a serious obstacle in using ferroelectrics as a media for high-density memory [9]. In order to understand the difference in the premature switching of the PZT films with increasing ac-voltage, the electrostatic pinning model was suggested [17, 26]. In this model, the existence of the "hidden" domain walls lying under the film's surface is postulated (Fig. 7). These walls are invisible at low ac-field and may only somewhat reduce the value of the collected signal. It is essential in our explanation that the field is highly localized near the contact area and continuously propagates into the film with increasing ac-voltage.

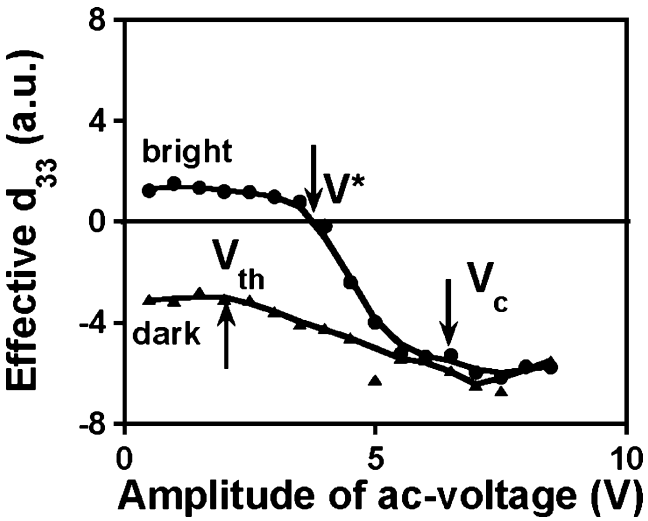

Fig. 6 Typical dependencies of the effective piezoelectric coefficient in PZT45/55 films on the amplitude of ac voltage for *bright* and *dark* domains [26]

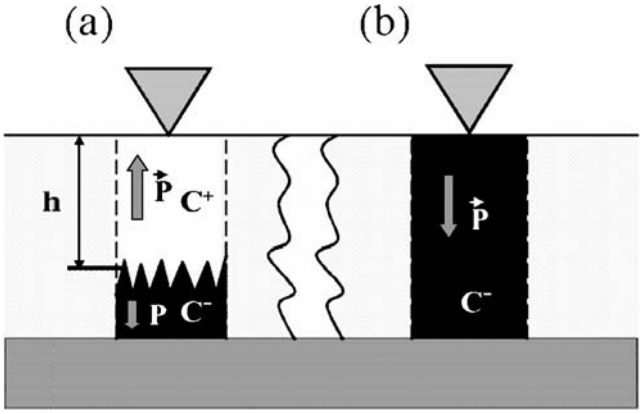

Fig. 7 Schematic of the domain configurations in the regions with bright contrast: (**a**) in as-grown film, (**b**) after depinning of charged domain boundary under increasing ac-field

The formation of bi-domain state in bright domains can be due to the presence of internal bias field, which manifests itself in self-polarization effect (see, e. g., [27, 28] and imprint [29]). Since the hidden 180° domain boundary corresponds to the "tail-to-tail" polarization configuration, it carries polarization charges and has to have a zig-zag shape. The depolarizing field of zig-zag boundary induces space-charge layer in the surrounding material. In PZT films, such space charge is likely to be due to trapped holes [30], so that the zig-zag boundary becomes pinned by electrostatic forces. Under a weak driving voltage, this boundary experiences only small field-induced shifts near its equilibrium position. Remarkably, the upward and downward shifts have to be different in magnitude, because the field induced by the PFM tip is non-uniform in the film thickness direction. Since the local value of this field is higher above the boundary than below it, the upward shift will be larger thus producing a larger (negative) domain contribution to the film piezoelectric response. The calculations show that this local domain wall motion results in a *decrease* of the effective d_{33} with increasing ac-voltage. When the local field at the domain boundary becomes larger than some threshold value E^*, it may be depinned from its equilibrium position. This leads to polarization reversal under the tip, so that the sign of local d_{33} changes to the opposite one. The threshold field can be derived with the simple formula [26]:

$$E^* = P_s \sin^2\theta / (\varepsilon_0 \varepsilon),$$

where θ is the zig-zag angle, P_S is the spontaneous polarization, and ε and ε_o are the relative dielectric permittivity and dielectric permittivity of vacuum, respectively. Thus local measurements, if properly done, can be used for the investigation of the dynamics of pinned domain walls in ferroelectrics.

6 Frequency dependence of local piezoelectric coefficients

Local piezoelectric properties of polycrystalline ferroelectric materials can be studied not only as a function of the applied ac field but also as a function of driving frequency. If the measurement frequency is much lower that the fundamental resonance frequency of the cantilever and there is no any spurious resonances in the system, the frequency dependence can be followed until several tens of kHz. In ferroelectrics, piezoelectric properties are generally frequency-dependent due to the large contribution of non-180° domain walls to the macroscopic piezoelectric response (see, e.g., excellent review by Damjanovic [31]). This typically leads to a slow relaxation of piezoelectric coefficients obeying linear-log dependence on frequency [31]. The comparison of the macroscopic and local results done on the same sol-gel PZT film with the Zr/Ti ratio 45/55 is shown in Fig. 8 for both in-plane and out-of-plane signals. The data are normalized to unity at low frequencies because the absolute values of the piezoelectric coefficients by PFM have not been determined. Macroscopic piezoelectric coefficient follow linear-log dependence with a very weak dispersion as typically observed in PZT thin films of the morphotropic phase boundary composition [32]. On the contrary, out-of-plane piezoelectric coefficient (roughly speaking analog of d_{33} in the macroscopic case) notably *increases* with frequency. To our surprise, we observed unexpectedly strong relaxation of lateral piezocoefficient (mainly proportional to d_{15} coefficient) that almost vanished between 10 and 100 kHz. The unusual behavior of out-of-plane component could be satisfactorily explained by depinning effect at high frequency similarly to that observed in the case of local piezoelectric nonlinearity (see Fig. 6). The strong dependence of lateral piezoelectric properties was found to be due to the slip motion of the cantilever relative to the moving piezoelectric surface [33]. In brief, at high frequencies the cantilever is not able to follow the piezoelectric surface (stick case) and slip has to occur. Therefore, we observed also a significant phase lag (Fig. 8b). The results were compared with the calculations performed using equation of motion of the cantilever taking into account both static and dynamic frictional forces [33]. Good correspondence has been found proving that the slip motion of the cantilever can imitate piezoelectric dispersion in local studies. In [33] it has been also noted that the big phase shift observed in the experiment cannot be fully explained by frictional phenomena. It is long time understood that the piezoelectric effect is, in general, represented by the real and imaginary components and piezoelectric loss may be essential, especially in inhomogeneous piezoelectrics [34]. Since piezoelectricity is a cross-coupling effect between dielectric and mechanical properties, both

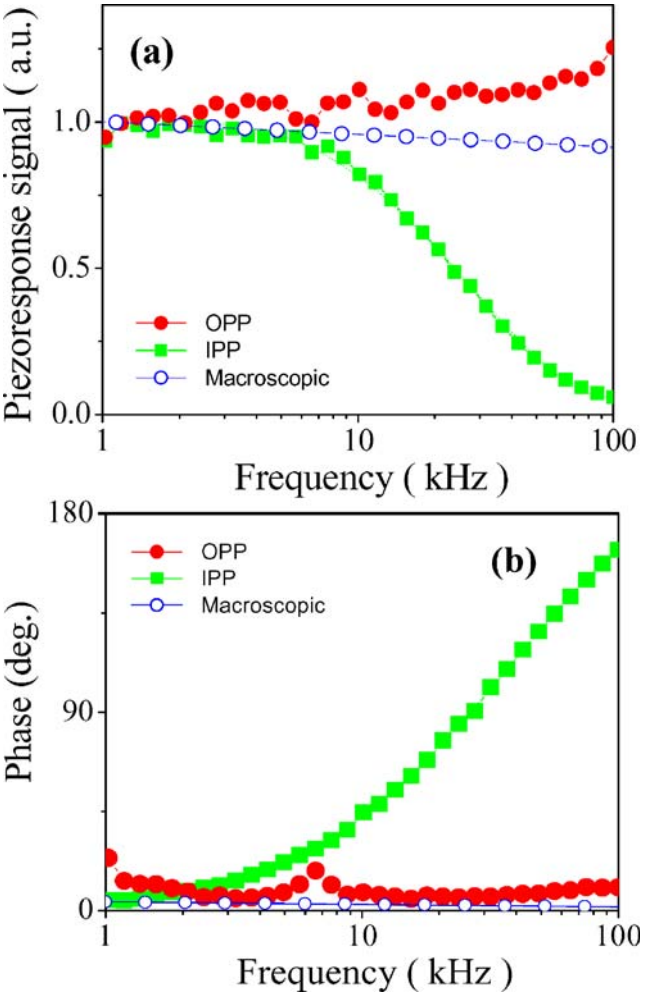

Fig. 8 Frequency dispersion of the in-plane and out-of-plane local piezoelectric signals in comparison with the macroscopic data. (**a**) normalized amplitude, (**b**) phase between the measured and driving signals. The measurements are taken on PZT30/70 films of the thickness 4 μm

mechanical and dielectric losses may contribute to piezoelectric loss. At low frequencies, the piezoelectric loss is typically explained by the dielectric loss, which may attain high values when the sample is conducting. In the case of Maxwell–Wagner relaxation (inhomogeneous piezoelectrics), the piezoelectric loss can be sufficiently high at low frequencies to explain the observed high local piezoelectric loss [35, 36]. It is important that the electric field applied to the PFM tip is highly inhomogeneous and decays very fast across the thickness of the sample. It means that upper layers see much higher local electric field, and, are more conducting that the layers that reside at some depth below the surface. This may result in an inhomogeneous conductivity, and, as a consequence, in a Maxwell–Wagner relaxation effect. Thus the additional phase shift between the driving voltage and the torsion of the cantilever can originate from the piezoelectric loss, i.e., from piezoelectric effect of the material itself.

7 Piezoelectric aging and fatigue

As was mentioned earlier, the local poling by PFM typically results in accelerated depoling and decrease of the piezoelectric coefficient with time. This depoling or piezoelectric aging is detrimental for MEMS applications of ferroelectric films because the total piezoelectric response and useful displacements are lower when the film is split into domains. The studies of macroscopic piezoelectric aging in PZT films have shown than not only depolarizing but also internal bias field is responsible for the accelerated depoling [37]. This field always points in one direction and is related either to the influence of electrodes (different work functions of both interfaces) or to non-uniform space charge distribution due to, e.g., diffusion of oxygen vacancies under the high-temperature processing of the films. Macroscopic piezoelectric aging in ferroelectric thin films has been reported in a number of papers (see, e.g., [37] and references therein). In local experiments, along with the d_{33} value, it is possible to visualize the lateral motion of the domain walls and the size of the poled area as a function of time. We present here the results of the measurements of local piezoelectric aging in PZT45/55 thin films [38]. For these experiments, two different regions were chosen. First, the rectangular area 300×300 nm^2 was polarized with a negative bias (−10 V) to create uniformly polarized areas. Further, the tip was positioned in the center of a large grain (region I) and +10 V pulse of 1 s duration was applied to switch the film mainly in the initial grain. In the second case (region II), the tip was located in the center of a small grain, so that the switching was initiated in several neighboring grains. Figure 9 shows the consequent evolution of the domain pattern with time.

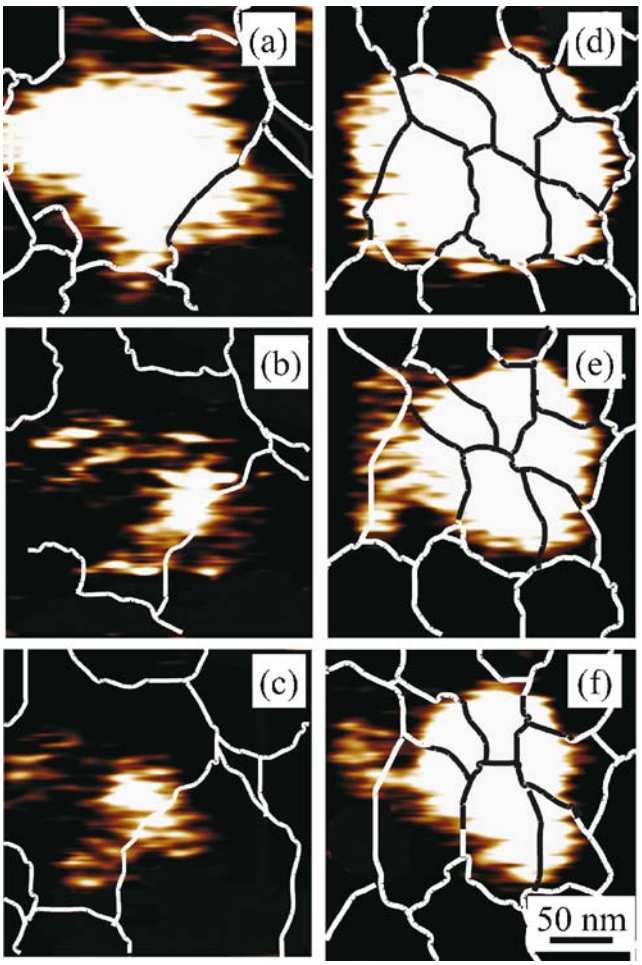

Fig. 9 Time evolution of written domain pattern in PZT45/55 films [38]. Switching is done in two different locations (*left column*: region I, *right column*: region II). The scans correspond to the following times after poling: (**a**), (**d**) –5 min, (**b**), (**e**) –20 min, (**c**), (**f**) –90 min

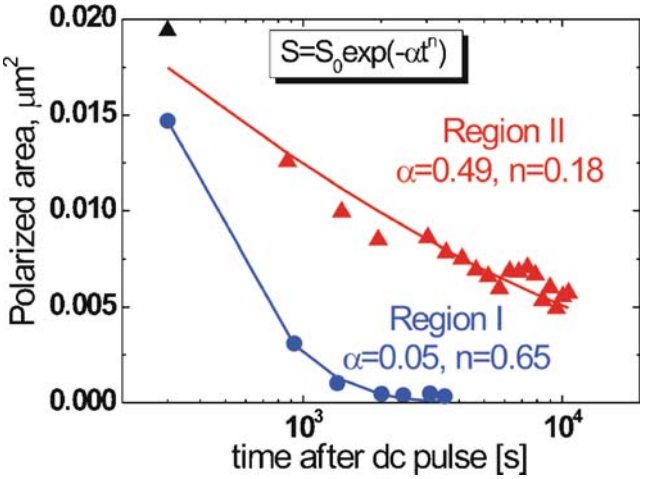

Fig. 10 Time evolution of the average piezoelectric coefficient in coarse-grain (*circles*) and fine-grain (*triangles*) locations in PZT45/55 films

It can be seen that in both regions the domain size decreases with time. When switching is done in a big grain this process is very fast, so that the domain almost disappears within 1 h. It is interesting that it is energetically favorable for the large domain to be split into small domains in this case. This indicates that the grain is inhomogeneous and increasing the domain wall energy is compensated by the energy gain from the pinning. It is confirmed by the fact that survived domain (see Fig. 9c) is located near the grain boundary. The evolution of the domain pattern in a fine-grain location is quite different, i.e., the local piezoelectric aging is much slower in this case. It is possible that the grain boundaries serve as additional pinning sites impeding the domain wall motion. This is similar to the vortex motion in the mixed state of superconductors where defects act as pinning centers [39].

Figure 10 quantifies the grain size effect on the relaxation of the piezoelectric coefficient after poling. The results were fitted with the so-called stretched exponential dependence:

$S=S_o\exp(-\alpha t^n)$, that is frequently used for the description of the stochastic processes in physics. For example,

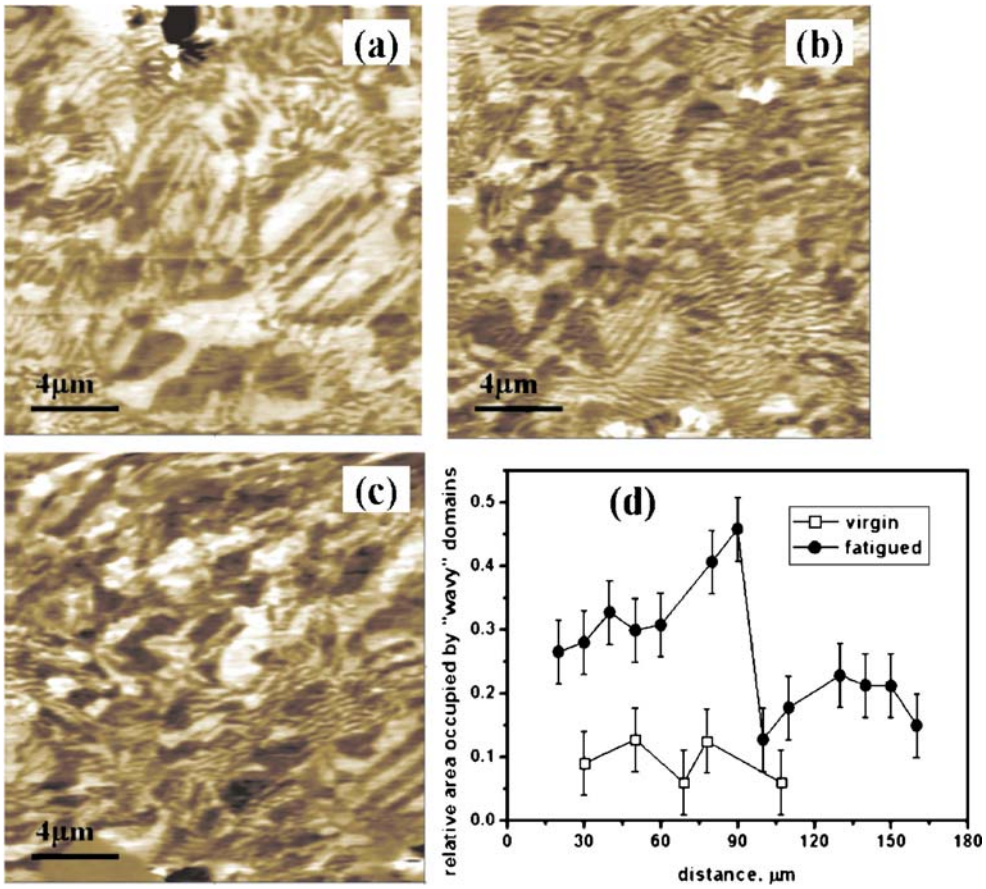

Fig. 11 Piezoresponse images obtained at different distances from the electrode [41]. (**a**) 20 μm, (**b**) 70 μm, and (**c**) 110 μm. (**d**) Relative área occupied by distorted domains as a function of the distance from electrode [42]

stretched exponential dependence with $n<1$ describes dispersive transport in amorphous semiconductors. In our measurements, the best fit was obtained with $n=0.65$ and 0.18 for coarse-grain and fine-grain areas, respectively. Thus the sidewise motion of the domains after poling can be discussed in terms of the random jumps of the segments of domain walls.

Besides aging, another important type of degradation is the polarization fatigue defined as a loss of switchable polarization during continuous domain switching. Fatigue is a general phenomenon that manifests itself in a similar way in thin films, polycrystalline ceramics, and single crystals [40], however, the microscopic mechanisms are drastically different. Besides microcracking (which is a priori a purely mechanical source of fatigue) the clamping of domains in preferred or random orientations has been assumed to be the major origin of fatigue. This clamping may occur at the domain walls via their interaction with defects or through the inhibition of seeding of new domains. The latter mechanism seems to dominate in ferroelectric thin films, where nucleation of opposite domains is inhibited by the injection of charge carriers from the electrode [40]. In ceramics, the pinning of domain walls seems to prevail and may be due to agglomerates of point defects (e.g., oxygen vacancies), defect dipoles, or space charges trapped near grain boundaries. Figure 11 illustrates domain changes induced by bipolar fatigue in commercial piezoceramics (PIC 151, PI Ceramic Lederhose, Germany) [41]. The measurements were done on the cross-sections of the ceramic samples subjected to fatigue at different distances from the electrode. It is seen that the fatigue behavior is mostly displayed near the electrode

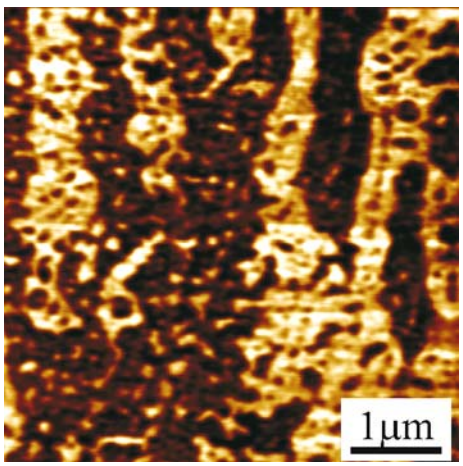

Fig. 12 Domain structure in PMN-20%PT single crystal illustrating a coexistence of "normal" micron-sized domains with remnants of polar clusters appearing due to random fields induced by B-site non-stoichiometry. The scan size is 5×5 μm^2

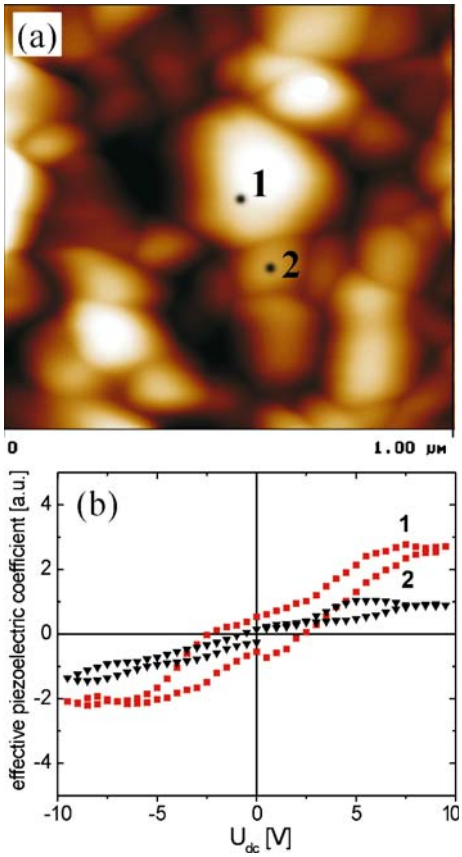

Fig. 13 Topography (**a**) and piezoresponse hysteresis (**b**) of PMN-PT film prepared by laser ablation [44]. Markers 1 and 2 (seen also on topography) denote different grains where the hysteresis was measured

where a large concentration of "wavy" stripe domains is observed. The appearance of these ferroelastic domains that are characteristic features of the fatigue process in ceramics is due to relieve of high mechanical stress appeared during polarization switching. Under normal circumstances, ferroelastic domains have to be oriented in certain crystallographic directions and be of a regular shape. However, near defects that can appear in the course of fatigue, bending of domain walls is likely to occur. Figure 11c shows the concentration of "wavy" domains as a function of distance from the electrode and clearly demonstrates that fatigue process is depth-dependent. Indeed, after the polishing and electrode redeposition, the initial properties of ceramics were restored.

8 Local properties of ferroelectric relaxors

Recently, ferroelectric relaxor materials such as $PbMg_{1/3}Nb_{2/3}O_3$ (PMN), $PbZn_{1/3}Nb_{2/3}O_3$ (PZN), and its solid solutions with $PbTiO_3$ became an object of increasing interest due to their high dielectric and electromechanical properties. Exceptionally high electrostrictive and piezoelectric strain of relaxor materials is especially attractive because of the absence of hysteresis, which is detrimental to high-precision actuators. It is widely accepted that unusual piezoelectric, ferroelectric and dielectric properties of relaxors are determined by the dynamics of nanoscale polar clusters that appear far above the temperature of the dielectric maximum. These clusters may coarsen and coalesce at low temperatures, but normal ferroelectric domains may develop only after poling with a dc bias. PFM is ideally suited for studying relaxors since the effective tip diameter can be as small as the polarization cluster size and the polarization value can be assessed through d_{33}. An example of the PFM study on PMN-0.2PT single crystals [42] is given in Fig. 12. The coexistence of rhombohedral domains (elongated strips) with remnants of polar clusters (small nanodomains embedded in between) is evident in this picture. It also illustrates the fractal nature of micron-sized domains when disorder is present. Nanodomains were shown to be important for the understanding of giant piezoelectric response in PZN-based materials [43]. In this work, nanodomains were only observed in PZN-0.045PT single crystals of certain crystallographic orientations, where the giant d_{33} is found.

In relaxor films, the switching into ferroelectric state was found to be influenced by the properties of the individual grains (due to their different orientation, chemical composition, mechanical stress, etc.). Typical topography and local piezoelectric hysteresis loops of PMN-0.1PT films are presented in Fig. 13 [44]. Grains exhibited slim hysteresis loop as expected for this composition at room temperature.

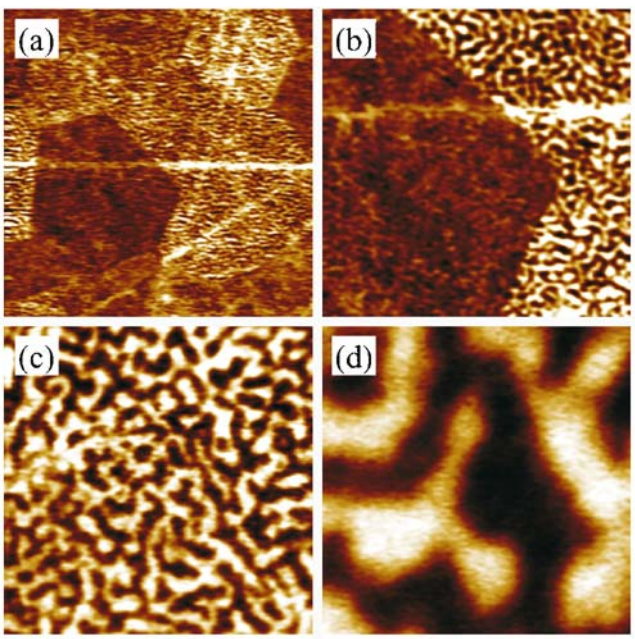

Fig. 14 PFM images of PLZT9.75/65/35 ceramics at different scales: (**a**) –12.5 μm, (**b**) –5 μm, (**c**) –2.5 μm, (**d**) –0.5 μm

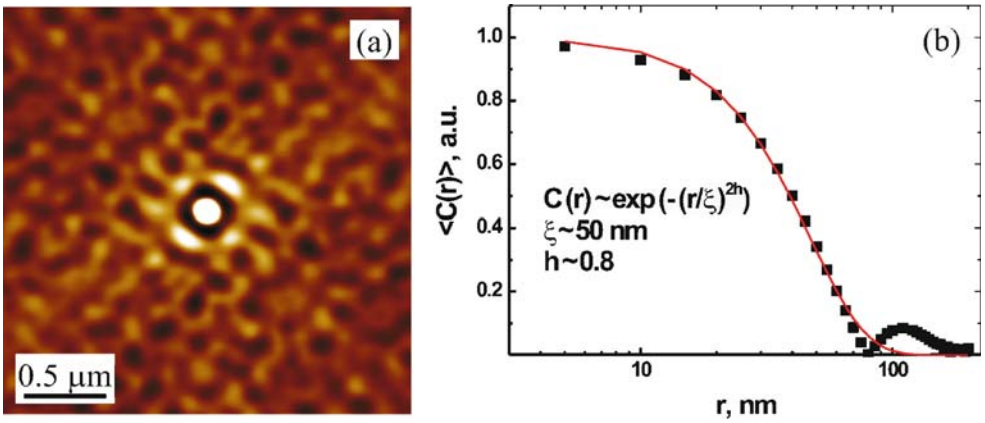

Fig. 15 Autocorrelation function of the piezoelectric image (**a**) and the averaged autocorrelation function vs. distance (**b**) in PLZT9.75/65/35 ceramics [46]

In addition, the contrast was found to depend on the grain size: the bigger the grain, the higher remanent d_{33} was observed. This proved that the grain size effect can be observed in relaxor films, even though the expected size of the polar clusters is much smaller than the grain size of the ceramic thin film. Some grains appeared spontaneously piezoelectric, proving the fact that the local relaxor-ferroelectric phase transition could take place. Two conclusions were made: (1) self-polarization can be found at the nanoscale in relaxor state, while it is hardly found in macroscopic measurements, and (2) since the piezoelectricity in relaxors is possible only under the bias field, the distribution of self-polarization represents also the distribution of internal field in these materials. Thus relaxor thin film on the microscopic level behaves as a nanocomposite, the macroscopic response of which can be derived by the averaging of local responses of the individual grains. Self-polarization was recently found also in pure PMN films

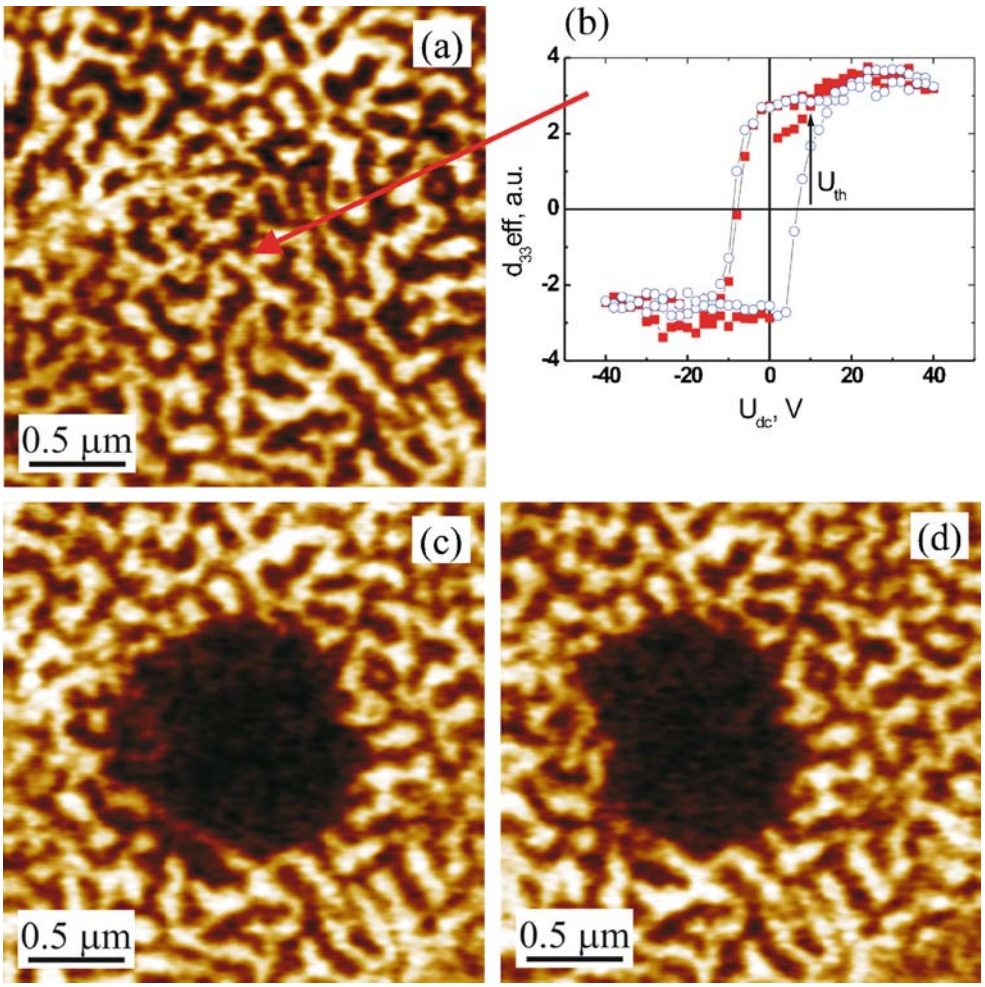

Fig. 16 (**a**) Initial domain structure of PLZT relaxor ceramics, (**b**) local hysteresis loop, (**c**) domain structure after application of 40 V to the center of the scan, (**d**) same image after relaxation during 7 h [46]

[45] proving that this unusual phenomenon in relaxor films is not related to local composition inhomogeneity due to fluctuations of $PbTiO_3$ content.

These results were complemented by the studies of domain structure in (Pb,La)(Zr,Ti)O_3 (PLZT) ceramics with high concentration of La [46]. The example of domain structure in PLZT with the concentration of La x=9.75% is shown in Fig. 14. Complex labyrinth structure of fingerprint-like domains reflects spatial inhomogeneities determined by both random field and random strains introduced with La doping. We applied a correlation analysis to the images and found that the images of the autocorrelation function (Fig. 15) are regular in two different directions revealing the local rhombohedral structure of these grains. Fitting of the average autocorrelation function gave the value of correlation length of about 50 nm. This value is several times larger that those expected for the polarization clusters and can be explained by the surface effect. Due to the surface boundary conditions and high electric field it is possible that polarization clusters are frozen and we observe only their fraction with large sizes.

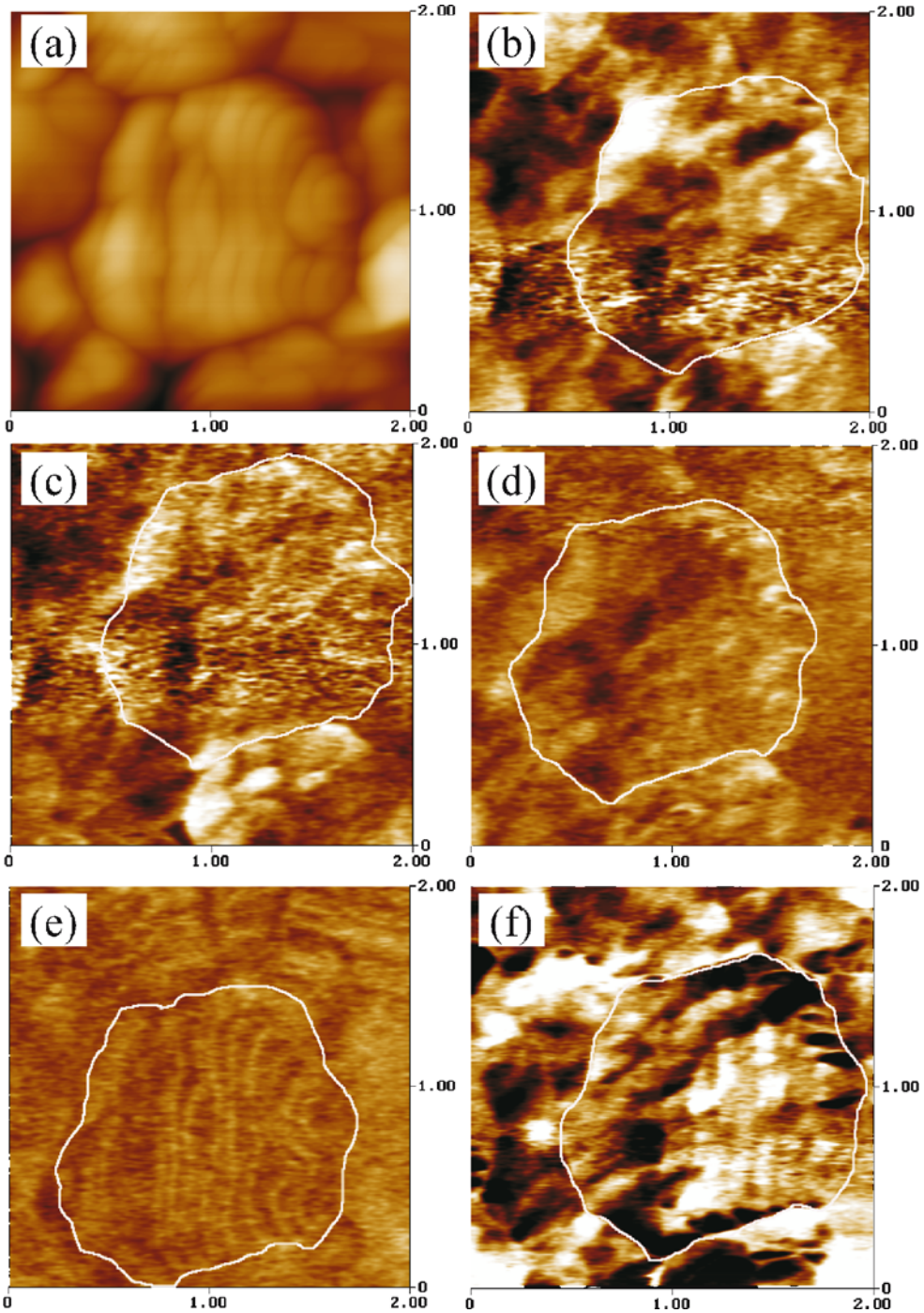

Fig. 17 Topography (**a**) and piezoresponse images (**b**–**f**) of the $BaTiO_3$ ceramics with 2.5% LMT doping at different temperatures: before heating at 295 K (**b**), 310 K (**c**), 330 K (**d**), 395 K (**e**) and after cooling back to room temperature (**f**) [47]

Figure 16 illustrates the poling effect on the nanodomain structure in PLZT 9.75/65/35. The measurements are done immediately after poling and after 7 h. It is seen that the induced ferroelectric state slowly relaxes with time back to the initial random domain structure where the local fields determined the polarization direction.

The intrinsic feature of relaxor ferroelectrics is the diffuse phase transition where the macroscopic polarization decays over a broad range of temperatures. This is generally attributed to the broad distribution of the relaxation time of polarization clusters some of which survive at the temperatures much higher than the nominal Curie point. Figure 17 shows a sequence of d_{33} images taken on a single grain of $BaTiO_3$ ceramics doped with 2.5% of $La(Mg_{1/3}Ti_{1/2})O_3$ at different temperatures both above and below Curie point [47]. This ceramics exhibit a diffuse transition shifted to lower temperature as compared to $BaTiO_3$. The relaxor behavior in this compound is due to the heterovalent substitutions by Mg^{2+} and La^{3+} at both A- and B-sites of the perovskite lattice. At room temperature, distinct polydomain structure is observed. Upon approaching the phase transition, the piezoresponse signal is becoming weaker while some domains disappear. However, even above the phase transition some nanodomains are observed pointing at the local inhomogeneity of relaxor ferroelectric. Interestingly, the domain structure reappeared after cooling (Fig. 17f) with some domains appeared at the same places. These places are related with the strong local electric field associated with defects or their agglomerates. Thus PFM allows following the dynamics of the diffuse phase transition when other imaging techniques fail because of the small size of nanodomains.

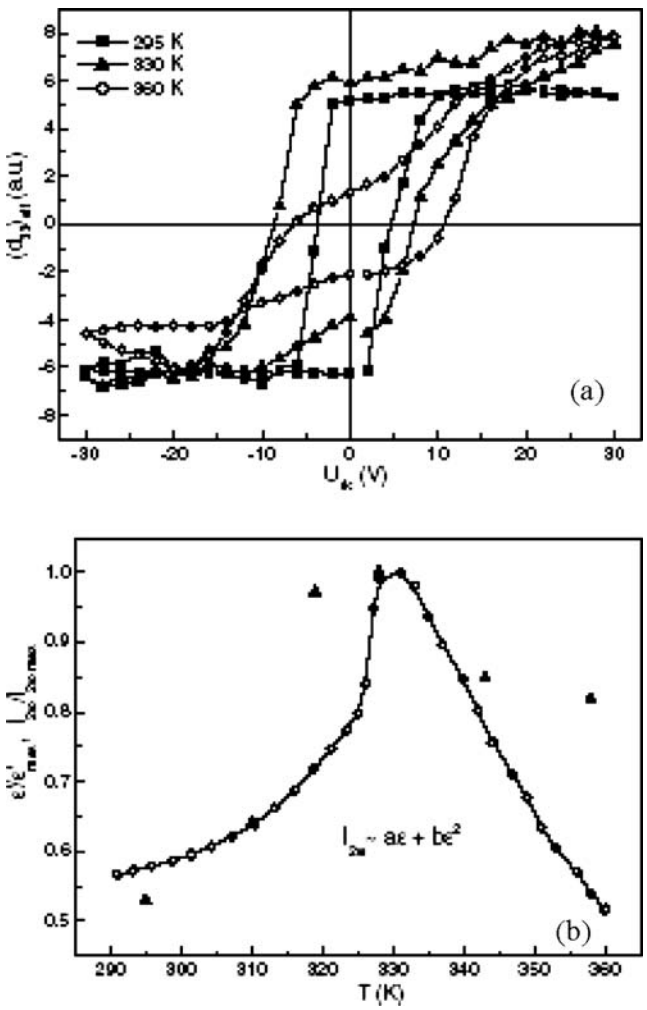

Fig. 18 (**a**) Local hysteresis loops taken in $BaTiO_3$: 2.5%LMT at different temperatures, (**b**) temperature dependence of the second harmonics of the electromechanical signal in comparison with the normalized dielectric permittivity [47]

Local piezoelectric hysteresis was measured at different temperatures in this ceramics (Fig. 18a). The measurements confirm decreasing of the induced piezoelectric response with increasing temperature in contradiction with macroscopic observation. Even above the phase transition, the hysteresis could be obtained but the shape of the hysteresis was propeller-like pointing to reappearing of the ferroelectric phase under the high electric field. Figure 18b illustrates the behavior of the second harmonics of the electromechanical signal that should consist of the mixture of electrostatic signal and electrostriction. The latter is proportional to the dielectric permittivity squared. The near coincidence of the two variables made us believe that the second harmonics may be useful for the evaluation of the local dielectric properties of polycrystalline materials.

9 Conclusions

In this work, the nanoscale characterization by piezoresponse force microscopy was performed on a number of polycrystalline materials that are important for piezoelectric applications. The local response was studied in thin films, ceramics and single crystals as a function of applied dc and ac fields, frequency, and grain size. The effect of the local polarization reversal under high ac-field was observed and analyzed. It is especially important for MEMS applications when the high driving voltages are expected. Local piezoelectric dispersion, nanoscale aging and fatigue were also studied by PFM. These measurements demonstrated that the structural and electronic defects may act as pinning centers for ferroelectric domain walls and thus influence nanoscale properties. Finally, local electromechanical properties of ferroelectric relaxors were presented. These measurements indicate that complex domain patterns that arise due to random electric fields and stresses in relaxors can be imaged with high spatial resolution by PFM. The examples were given for several classes of relaxors including PLZT, PMN-PT and $BaTiO_3$ families.

Acknowledgements The authors wish to thank Dr. N. Pertsev and Dr. S. Vakhrushev for continuing collaboration and numerous discussions regarding piezoelectric nonlinearity and PFM results in ferroelectric relaxors. We also express our gratitude to Prof. D. Lupascu for providing the samples and discussion of piezoelectric fatigue in ceramics. Prof. A. Safari and Dr. A. Sternberg are acknowledged for providing the samples used in this study. I. K. B. and D. A. K. acknowledge the financial support from the Portuguese Science and Technology Foundation (FCT) via grants SFRH/BPD/12031/2002 and SFRH/BD/22391/2005, respectively. Part of the work is performed within NOE 'FAME' (NMP3-CT-2004-500159).

References

1. J.F. Scott, Ferroelectr. Rev. **1**, 1 (1998)
2. D.L. Polla, L.F. Francis, MRS Bull. **59**, July (1996)
3. A. Gruverman, O. Auciello, H. Tokumoto, Annu. Rev. Mater. Sci. **28**, 101 (1998)
4. L.M. Eng, S. Grafstrom, C. Loppacher, F. Schlaphof, S. Trogisch, A. Roelofs, R. Waser, Adv. Solid State Phys. **41**, 287 (2001)
5. *Nanoscale Phenomena in Ferroelectric Thin Films*, ed. By Seungbum Hong (Kluwer, 2004)
6. M. Alexe, A. Gruverman (ed.), *Nanoscale Characterization of Ferroelectric Materials* (Springer, Berlin Heidelberg New York, 2004)
7. S.V. Kalinin, A. Rar, S. Jesse, in *IEEE Trans. Ultrason. Ferroelectr. & Freq. Control: Invited Paper in Special Issue on Nanoscale Ferroelectrics*, ed. By A. Gruverman, A.L. Kholkin (December 2006)
8. A.L. Kholkin, A. Roelofs, S.V. Kalinin, A. Gruverman, in *Electrical and Electromechanical Phenomena on the Nanoscale by Scanning Probe Microscopy*, ed. By S.V. Kalinin, A. Gruverman (Springer, Berlin Heidelberg New York, 2006)
9. C. Ahn, T. Tybell, L. Antognazza, K. Char, R.H. Hammond, M.R. Beasley, Ø. Fischer, J.-M. Triscone, Science **276**, 1100 (1997)
10. P. Güthner, K. Dransfeld, Appl. Phys. Lett. **61**, 1137 (1992)
11. K. Franke, Ferroelectr. Lett. **19**, 35 (1995)
12. C. Durkan, D.P. Chu, P. Migliorata, M.E. Welland, Appl. Phys. Lett. **76**, 3666 (2000)
13. D.V. Taylor, K.G. Brooks, A.L. Kholkin, D. Damjanovic, N. Setter, in *Proc. of the 5th Int. Conf. on Electronic Ceramics and Applications*, ed. by J.L. Baptista (Aveiro, Portugal, 1996), v. 1, p. 341
14. A.L. Kholkin, E.K. Akdogan, A. Safari, P.-F. Chauvy, N. Setter, J. Appl. Phys. **89**, 8066 (2001)
15. A.L. Kholkin, E.L. Colla, A.K. Tagantsev, D.V. Taylor, N. Setter, Appl. Phys. Lett. **68**, 2577 (1996)
16. Y. Zhang, I.S. Baturin, E. Aulbach, D.C. Lupascu, A.L. Kholkin, V.Y. Shur, J. Rödel, Appl. Phys. Lett. **86**, 012910 (2005)
17. V.V. Shvartsman, N.A. Pertsev, J.M. Herrero, C. Zaldo, A.L. Kholkin, J. Appl. Phys. **97**, 104105 (2005)
18. M.I. Molotskii, M.M. Shvebelman, Philipp. Mag. **85**, 1637 (2005)
19. A.L. Kholkin, I.K. Bdikin, V.V. Shvartsman, A. Orlova, D.A. Kiselev, A.A. Bogomolov, Mater. Res. Soc. Proc. **838E**, O7.6 (2005)
20. A.L. Kholkin, Ch. Wuethrich, D.V. Taylor, N. Setter, Rev. Sci. Instrum. **67**, 1935 (1996)
21. S.V. Kalinin, A. Gruverman, D.A. Bonnell, Appl. Phys. Lett. **85**, 795 (2004)
22. A. Wu, P.M. Vilarinho, V.V. Shvartsman, G. Suchaneck, A.L. Kholkin, Nanotechnology **16**, 2587 – 2595 (2005)
23. H. Maiwa, J.-P. Maria, J.A. Christman, S.-H. Kim, S.K. Streiffer, A.I. Kingon, Integr. Ferroelectr. **24**, 139 (1999)
24. A.L. Kholkin, Ferroelectrics **221**, 219 (1999)
25. A.L. Kholkin, Ferroelectrics **258**, 209 (2001)
26. V.V. Shvartsman, A.L. Kholkin, N.A. Pertsev, Appl. Phys. Lett. **81**, 3025 (2002)
27. A.L. Kholkin, K.G. Brooks, D.V. Taylor, S. Hiboux, N. Setter, Integr. Ferroelectr. **22**, 525 (1998)
28. G. Suchanek, G. Gerlach, Yu. Poplavko, A.I. Kosarev, A.N. Andronov, Mater. Res. Symp. Proc. **655**, C.7.7.1 (2003)
29. W.L. Warren, D. Dimos, G.E. Pike, B.A. Tuttle, M.V. Raymond, R. Ramesh, J.T. Evans, Appl. Phys. Lett. **67**, 866 (1995)
30. A.L. Kholkin, N. Setter, Appl. Phys. Lett. **71**, 2854 (1997)
31. D. Damjanovic, Rep. Prog. Phys. **61**, 1267 (1998)
32. D. Damjanovic, D.V. Taylor, A.L. Kholkin, M. Demartin, K.G. Brooks, N. Setter, Mater. Res. Soc. Proc. **459**, 15 (1997)
33. I.K. Bdikin, V.V. Shvartsman, S.-H. Kim, J. Manuel Herrero, A.L. Kholkin, Mater. Res. Soc. Symp. Proc. **784**, C11.3 (2004)
34. R. Holland, IEEE Trans. Sonics Ultrason. **SU-14**, 18 (1967)
35. K. Hamano, Y. Yamaguchi, Ferroelectrics **42**, 23 (1982)
36. D. Damjanovic, M. Demartin Maeder, P. Duran Martin, C. Voisard, N. Setter, J. Appl. Phys. **90**, 5708 (2001)
37. A.L. Kholkin, A.K. Tagantsev, E.L. Colla, D.V. Taylor, N. Setter, Integr. Ferroelectr. **15**, 317 (1997)
38. V. Shvartsman, A.L. Kholkin, Ferroelectrics **286**, 291–299 (2003)
39. J.I. Martin, M. Velez, J. Noguez, I.K. Schiller, Phys. Rev. Lett. **79**, 229 (1997)
40. A.K. Tagantsev, I. Stolichnov, E.L. Colla, N. Setter, J. Appl. Phys. **90**, 1387 (2001)
41. V.V. Shvartsman, A.L. Kholkin, C. Verdier, D.C. Lupascu, J. Appl. Phys. **98**, 094109 (2005)
42. V.V. Shvartsman, A.L. Kholkin, Phys. Rev. B. **69**, 014102 (2004)
43. I.K. Bdikin, V.V. Shvartsman, A.L. Kholkin, Appl. Phys. Lett. **83**, 4232 (2003)
44. V.V. Shvartsman, A. Yu. Emelyanov, A. Safari, A.L. Kholkin, Appl. Phys.Lett. **81**, 117 (2002)
45. V.V. Shvartsman, A.L. Kholkin, M. Tyunina, J. Levoska, Appl. Phys. Lett. **86**, 222907 (2005)
46. V.V. Shvartsman, A. Orlova, D. Kiselev, A.A. Bogomolov, A. Sternberg Appl. Phys. Lett. **86**, 202907 (2005)
47. A.N. Salak, V.V. Shvartsman, M.P. Seabra, A.L. Kholkin, J. Phys. Cond. Matt. **16**, 2785 (2004)